L.A. Sgro
University Naples
Italia

Particles < 3 nm in different combustion systems: UV-Vis extinction, atomic force microscopy and differential mobility analysis

d<3 nm Particles in Different Combustion Systems: UV-visible Extinction, Atomic Force Microscopy and Electrospray-Differential Mobility Analysis

L. A. Sgro[1], G. Basile[1], A. C. Barone[1], A. D'Anna[1], P. Minutolo[2], A. Borghese[3], A. D'Alessio[1]

[1]Dipartimento di Ingegneria Chimica
Universita degli Studi di Napoli Federico II
Piazzale Tecchio 80, 80125 Napoli, Italy

[2]Istituto di Ricerche sulla Combustione, CNR
Piazzale Tecchio 80, 80125 Napoli, Italy

[3]Istituto di Motori, CNR
Via Marconi 8, 80125 Napoli, Italy

Introduction

It is of interest to measure the size distribution of nanoparticles produced in combustion systems to better understand how particle size may affect human health, the radiation balance of the atmosphere and to study the formation of larger soot particles. We present results comparing the size evaluation of inception particles in highly controlled premixed ethylene air flames using three different measurement techniques: *in situ* UV-visible extinction and scattering, *extra situ* analysis by Atomic Force Microscopy (AFM) and Electrospray – Dynamic Mobility Analysis (E-DMA). All three techniques are sensitive to particles in the nanometer size range, also under 3 nm, which is below the limit of detection of commercially available particle sizing instrumentation. Previous work using UV-visible optical techniques (1), transmission electron microscopy (2, 3), and thermophoresis sampling (4) indicate the presence of d<3 nm particles produced in combustion processes, though their formation mechanisms are not yet well understood. Optical techniques are advantageous since they do not induce significant sampling errors with respect to *extra situ* techniques, but the optical properties of particles are needed (5). Comparison of various measurement techniques in well controlled and characterized combustion experiments is important in diagnostic development for sizing inception particles formed in combustion. UV-visible spectral extinction measurements are also used to simultaneously quantify the amount of d<3 nm and larger soot particles in the exhausts of practical systems.

Experimental Techniques

We compare the size analysis evaluated by three measurement techniques, UV-visible extinction spectra, AFM, and E-DMA, of particles generated in premixed ethylene air flames. Premixed flames are an excellent source of particles as they operate at steady state and are well controlled and characterized. Temperature and species concentrations vary only along the flame axis, and can be well-measured. In addition, they offer a rather large experimental space to make measurements in the post-flame region where particulate matter is formed. The light emission from a plasma created by focusing the 1064 nm beam from a pulsed Q-switched Nd:Yag laser in air provide a broadband UV-visible light source for the extinction measurements (Fig. 1) (6). For scattering measurements, the fourth harmonic Nd:Yag laser at 266 nm was used directly as the light source, and the signal was measured at 90 degrees.

The extinction spectra presented in this work are an excess extinction attributed to particles that remains after the calculated extinction from the gas phase products in the flame has been subtracted. The concentration of gas phase products is calculated using a detailed chemical kinetic mechanism for ethylene air combustion reactions and the CHEMKIN premixed flame code (7). The absorption from gas phase species is calculated from the concentration and their measured absorption cross sections; most of the absorption from gas phase species comes from CO_2 at high temperature (8).
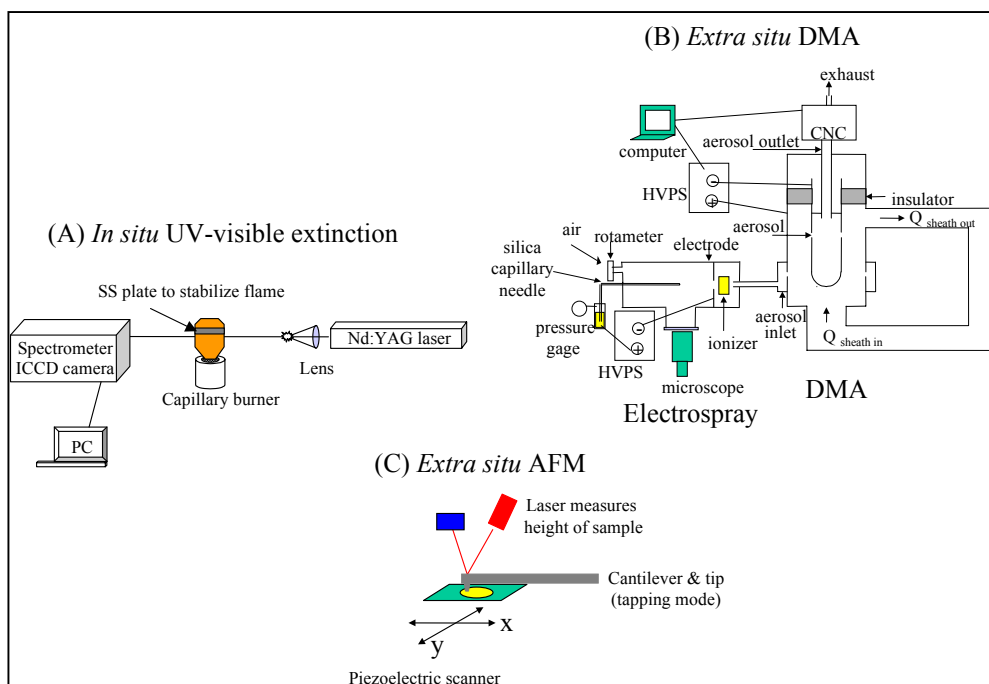
Figure 1: Experimental techniques used to measure the size of inception particles in premixed flames.

Analysis using AFM was performed on particles collected by thermophoresis on a cold mica disc rapidly inserted into the flame. The surface of the sample is mapped out in angstrom-nanometer resolution by moving the sample under a vibrating cantilever beam, while both the beam position, and the x-y position of the sample are precisely measured. The analysis was done with the Digital Instruments Nanoscope IIIa ® AFM operating in tapping mode. The analysis methodology was optimized for the type of sample substrate, sampling time, and the construction of the AFM tip. Further experimental details can be found elsewhere (9).

The E-DMA measurements were performed on condensed combustion water samples collected by cooling extracted combustion products below the condensation point of water; this technique has been studied previously and is thought to be a good method for isolating particles of a few nanometers in size from other flame products (10). The methodology for E-DMA analysis follows closely the work of Kaufmann, *et al.* (11, 12) who used the same technique to measure the size of large biomolecules in the nanometer and sub-nanometer size range. The electrospray source is used to dry and charge particles contained in the condensed combustion water samples and to entrain the products of electrospray in a stream of CO_2 that flows directly to the entrance slit of a DMA. The DMA classifies the charged particles as a function of their electrical mobility, which is proportional to size. A condensation nucleus counter (CNC) is used as a detector at the exit of the DMA. All three components (electrospray, DMA, and CNC) are optimized drying, sizing, and counting particles in the nanometer to sub-nanometer size range following the work of Fernandez de la Mora, *et al.* (13-16). More details explaining the E-DMA technique applied to hydrosols collected from rich combustion conditions can be found elsewhere (17).

Results

Without making any assumptions about the optical properties of particles, it can be seen that fuel rich premixed flames produce mainly two types of scatterers/absorbers by plotting the raw scattering and extinction measurements in the UV (Fig. 2). The first part of the curve is linear; it can be due to Rayleigh scatterers whose diameter is constant since $Q_{vv}/K_{ext} \propto d^3$, where d is the particle diameter (Fig. 2). The second part of the curve shows a much stronger scattering signal, and the curve is non-linear, indicating an increasing size of the particles which absorb/scatter the laser light. The Rayleigh equations (Fig. 2) with known or assumed refractive index, m, are used to elaborate particle size and number concentration from extinction, K_{ext}, and scattering, Q_{vv}, measurements. In this study, we used the refractive index, $m(266 \text{ nm}) = 1.4 + 0.08\,i$, for the visible-transparent particles; more details on the optical techniques used and the evaluation of refractive index for the d<3 nm particles can be found in earlier studies (1, 5, 18, 19).

$$K_{ext} = \frac{\pi^2}{\lambda_o} \left\{ \frac{m^2-1}{m^2+2} \right\}^2 N d^3$$

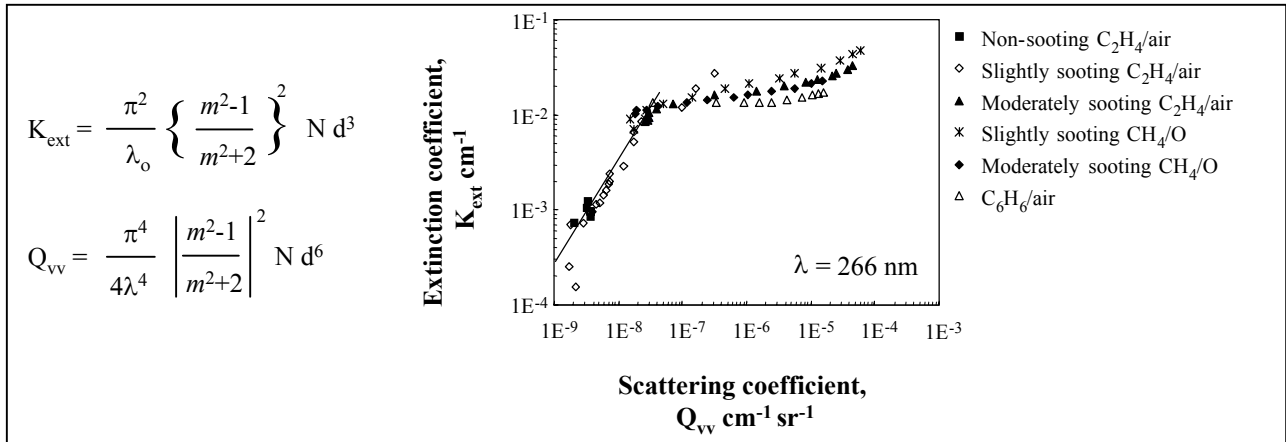$$Q_{vv} = \frac{\pi^4}{4\lambda^4} \left| \frac{m^2-1}{m^2+2} \right|^2 N d^6$$

Figure 2: Excess extinction and scattering attributed to particulate in the flame after the contribution from gas phase combustion products is subtracted. Different symbols show measurements taken in different flames, and different points with the same symbol represent measurements taken at various heights above the burner surface.

More information to characterize the particles is obtained by collecting extinction spectra. The form of the UV-visible extinction curves changes strongly as a function of fuel to air or C/O ratio, and can be used to indicate the size/type of particles present (18, 20). In slightly rich, non-sooting, blue flames no visible absorption is measured, and the spectra (Fig. 3 A) is associated with particles of approximately d=2.5 nm, evaluated by combined extinction and scattering measurements. In these non-sooting flames, the size of these particles remains constant with increased flame residence time. Increasing the amount of fuel or C/O ratio produces products with extinction spectra with significant, growing absorption in the visible (Fig. 3 B and C); these spectra are associated with larger, more graphitic particles, which grow in size with flame residence time (18).
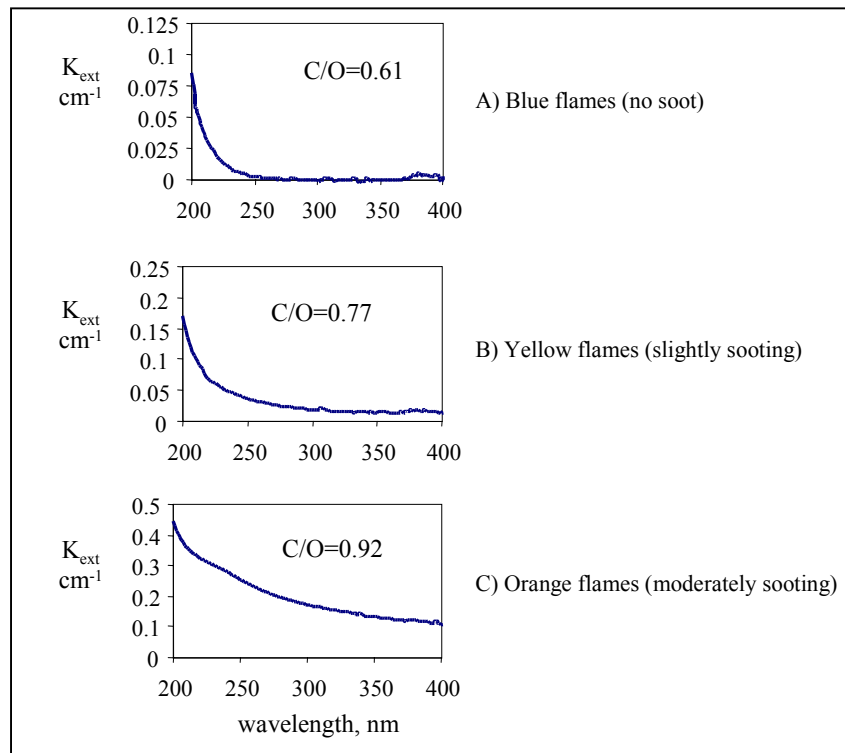

Figure 3: Typical extinction spectra for various ethylene air flames.

Figure 4 replots the same extinction spectra for the C/O=0.92 ethylene air flame (Fig.3(C)), showing explicitly the contributions of the two main types of particles (nanoparticles and soot). The contribution to the total extinction curve from the d=2-3 nm nanoparticles was measured at a flame height just after the flame front, before visual light absorbing soot-like

particles are formed (see the curve labled 'd<3nm' in Fig. 4). By subtracting the nanoparticle contribution from the total extinction curve, the spectrum attributed to the more graphitic soot-like particles is obtained (see the curve labeled 'soot' in Fig. 4). The shape of the extinction curve attributed to the soot-like particles obtained by subtraction in figure 4 is similar to the extinction spectrum measured in pyrolysis oil experiments, in which soot is mainly formed without the presence of nanoparticles.
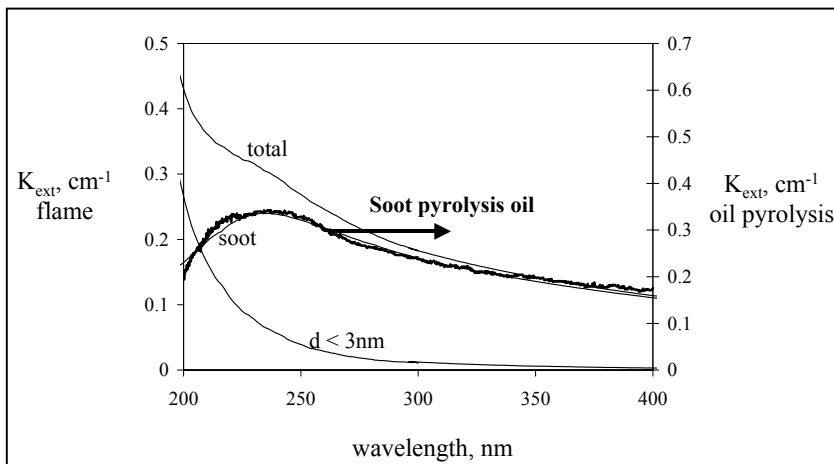

Figure 4: Extinction spectrum for the C/O=0.92 flame separated into two spectra of the main types of particles observed: the spectrum attributed to nanoparticles (labled d<3 nm), and the spectrum of soot-like particles (labled soot). The extinction spectrum of soot-like particles has a shape similar to that of soot produced in pyrolysis oil experiments (thicker curve).

Similar to the size analysis using the UV-visible optical techniques, AFM results show that in slightly rich flames, only nanoparticles are detected, with a particle distribution centered around d=3 nm. In richer flames, the size distribution is more bimodal, and both nanoparticles and larger particles are observed (Fig. 5).
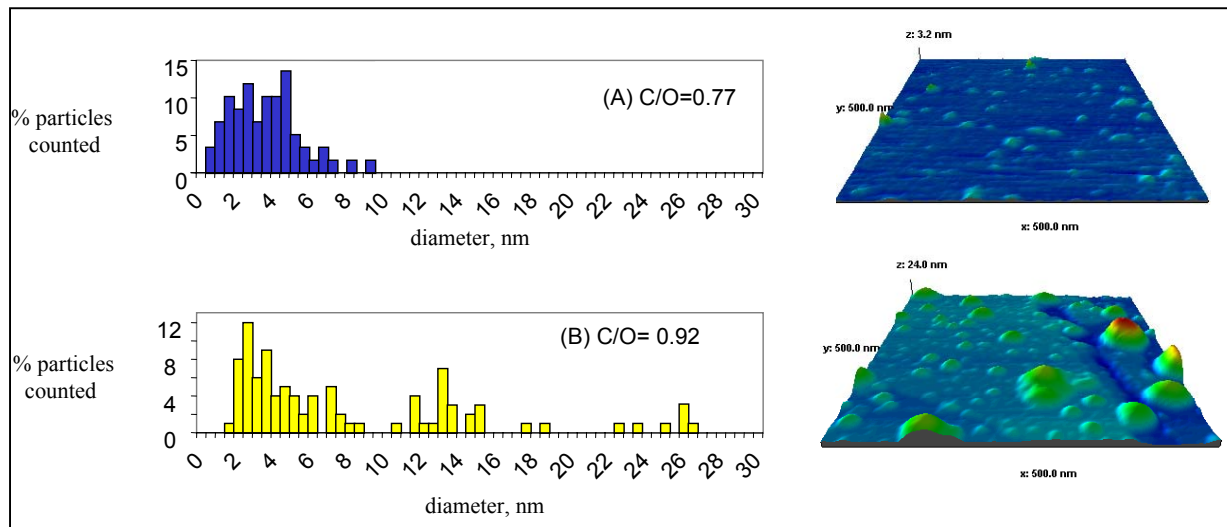

Figure 5: Particle size distributions evaluated with AFM on thermophoretic samples from premixed ethylene air flames.

The E-DMA analysis of combustion water samples resulted in a particle size distribution as shown in Figure 6. This size distribution was taken with the DMA running at conditions that give a resolution of +/- 10 % in size. The distribution is similar to that measured by AFM for the C/O=0.77 flame.
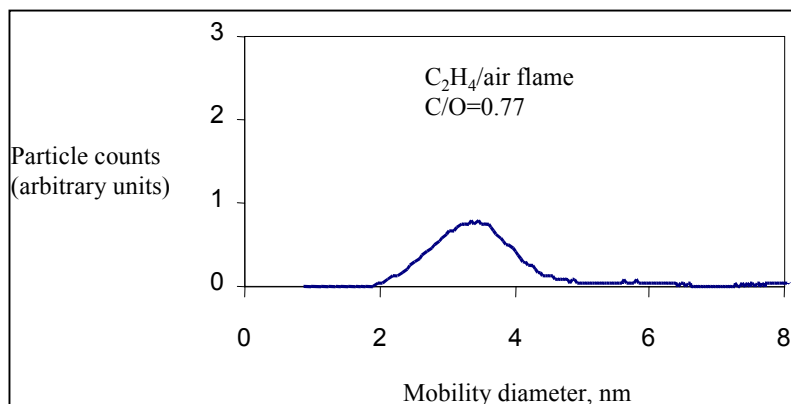
Figure 6: Size distribution determined by E-DMA for a condensed water sample collected from premixed flames.

Figure 7 plots the mean diameter as evaluated by all three techniques for the C/O=0.77 ethylene air flame. The agreement is quite good indicating that the optical properties and elaboration of the optical signals is sound and that the external sampling techniques do not significantly alter the size distribution of sampled particles.
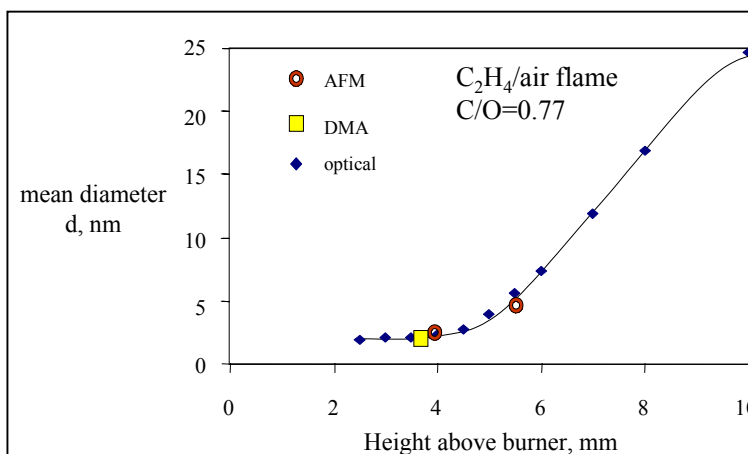

Figure 7: Particle size evaluated by three different techniques, UV-visible extinction and scattering, AFM and E-DMA.

The number concentration and mean diameter of particles present can be evaluated using the Rayleigh approximations (listed in Fig. 2), and the coagulation coefficient can be calculated from the particle number concentration and its derivative in time. Figure 8 illustrates that the coagulation rate changes several orders of magnitude along the axis of the flame. Particles measured just after the flame front which do not absorb visible light, and have diameters under 3 nm coagulate at a rate orders of magnitude slower than the larger soot particles, which absorb strongly in the visible and are observed later in the flame, or at higher heights above the burner surface.

Following the work of Narsimhan and Ruckenstein (21), we used a numerical model to predict the coagulation rate of particles in the premixed flames studied. The model accounts for the Van der Waals attraction and Born repulsion in the calculation of the rate of collision and subsequent coagulation. In general, coagulation of two particles after collision occurs if the kinetic energy of the particles is lower than their interaction potential.

$$\text{Coagulation Coefficient} = - \frac{dN}{dt} \frac{1}{N^2}$$

C_2H_4/air flame
C/O=0.77

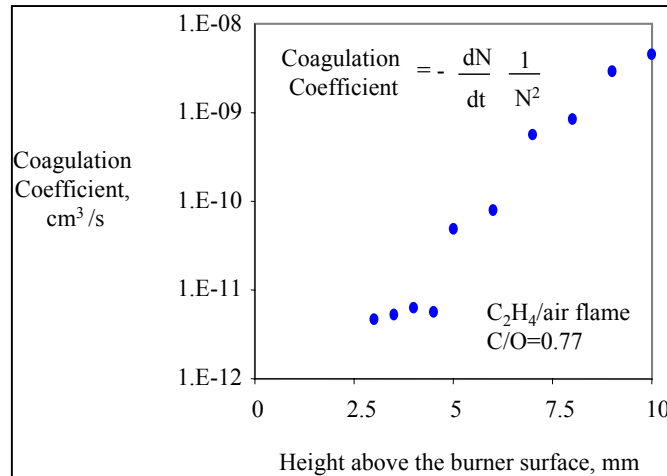Coagulation Coefficient, cm^3/s

Height above the burner surface, mm

Figure 8: Coagulation coefficient elaborated from scattering and extinction measurements (5).

Figure 9 replots the coagulation coefficients determined from extinction and scattering measurements (same data from Fig. 8) along with those predicted by the numerical model as a function of particle size. The coagulation coefficients calculated for three different Hamaker constants are plotted in figure 9, assuming that the particles will behave in an interaction similar to graphite, benzene, or an aliphatic structure. There is a small window of particle size of just a few nanometers in which the coagulation rate predicted by the model changes several orders of magnitude. For a particle composed of graphite, the window in which the coagulation coefficient changes greatly is very tight, encompassing d=0.2-0.8 nm, while for benzene and aliphatic structures the window shifts to larger size particles and the change is less steep.

The experimental data fall in between the model predictions using an Hamaker constant considering the particles are comprised of benzene and that for an aliphatic structure (Fig. 9), which is in agreement with previous thoughts about their chemical structure. The 2-3 nm particles formed in hydrocarbon combustion are thought to be comprised of aromatics with no more than 2-3 rings linked in a polymer-like way by aliphatic bonds possibly containing oxygen as deduced by their optical signatures. In contrast, soot particles, with typical sizes of 20-50 nm, have a more graphitic structure, and would be expected to have a coagulation rate closer to that predicted by the gas kinetic limit. The chemical/physical transformation of nanoparticles to soot particles is an aromatization process, which accompanies the coagulation or coalescence. The agreement between the numerical coagulation model and the experimental data suggests that small combustion-generated particles have properties which place them in the window where the repulsive forces during an interaction are greater than the attractive forces, thus reducing greatly their collision efficiency and rate of coagulation. As the particles grow in size and become more aromatic, they move quickly out of this window, and their collision efficiency approaches that of the gas kinetic limit where every interaction results in a collision.

graphite (A=$5E^{-12}$)

benzene (A=$5E^{-13}$)

aliphatic (A=$1E^{-13}$)

T=1800K

Gas Kinetic Limit

Coagulation Coefficient cm^3/s
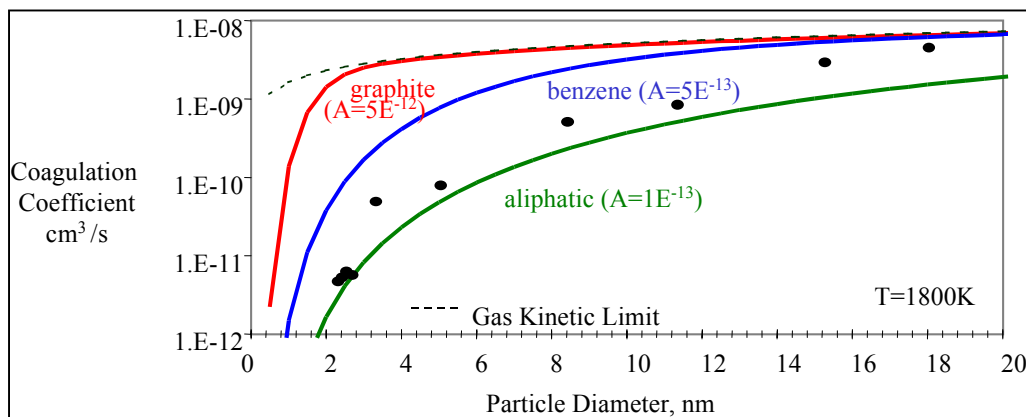
Particle Diameter, nm

Figure 9: Coagulation coefficients calculated from extinction and scattering measurements (symbols) and those predicted by a numerical coagulation model (lines) for different values of the Hamaker constant, A.

The same UV-visible optical techniques used to measure nanoparticles and soot in situ in laboratory premixed flames can also be applied to practical combustion systems (22, 23). After interfering species in the gas phase (most notably, NO, NO_2 and SO_2) are subtracted from extinction curves taken in the diluted exhausts of practical systems, the remaining extinction spectra in the UV-visible is, in some operating conditions, similar to those measured in premixed flames. Fig 10 shows the similarity between the measured extinction spectra in diluted exhausts overlaid on those observed in ethylene air flames.
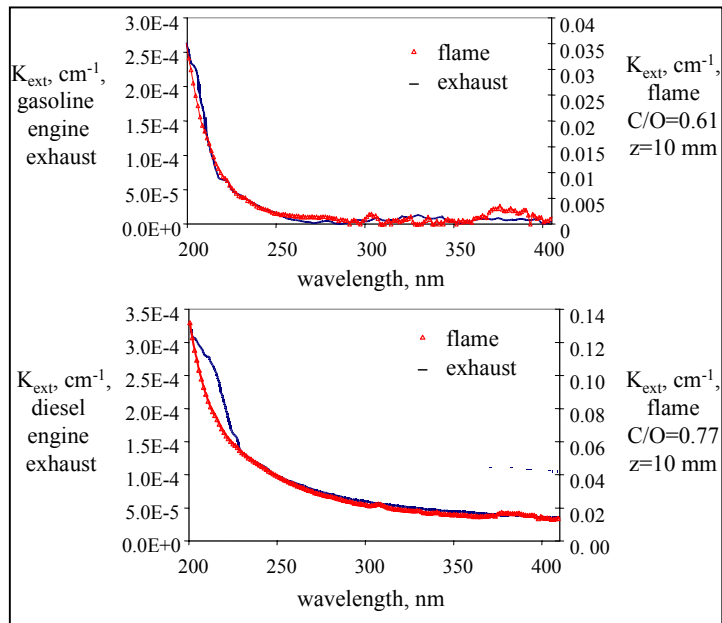

Figure 10: Extinction spectra from engine exhausts compared to those from premixed ethylene air flames

Given the similarity of the extinction curves, the total broadband spectra can be separated into two additive extinction curves: one attributed to soot and the other to the d=2-4 nm particles, as was illustrated in Fig. 4 for data collected in premixed flames. Figure 11 shows the estimated concentrations of d<3 nm particles and soot particles; the error bars in the concentration data take into account the range of variability of the results observed at different operating loads.
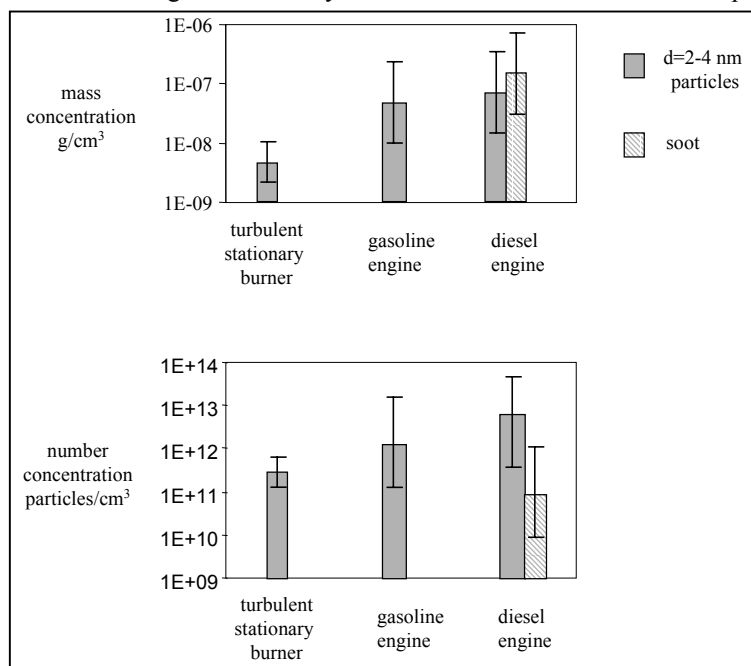

Figure 11: Mass and number concentration of d<3 nm particles and soot particles emitted in practical combustion systems as evaluated by UV-visible extinction spectroscopy.

Table 1 lists the assumption s used to calculate the concentrations presented in figure 11 from extinction measurements. Nanoparticles were observed in higher concentrations for the engine exhausts than for stationary burners. Soot particles were observed only in the diesel exhaust emissions.

Table 1: Assumptions used to quantify soot and nanoparticles from UV-vis extinction in various combustion exhausts at different loads.

	Soot	Nanoparticles
Diameter, d	20 nm	3 nm
Density	1.8 g/cm^3	1 g/cm^3
Refractive index (m (λ)= n + k i)		
λ = 266 nm	-	m(266 nm) = 1.4+ 0.08 i
λ = 200 nm	-	m(200 nm) = 1.1 + 0.47 i
λ = 500 nm	m(500 nm) = 1.5 + 0.56 i	

Conclusions

Particles with diameter, d<3 nm, are formed in high temperature combustion, and are detected by three different techniques: UV-visible extinction and scattering, AFM, and E-DMA. The *extra situ* sampling methods do not significantly alter the size distribution of d<3 nm particles as they compare well with the average size obtained from *in situ* UV extinction and scattering measurements. Since the ethylene air flames used to produce these particles contain no sulfur, the results strongly show that nanoparticles produced in combustion processes can be of a different chemical nature than condensed sulfates.

Combustion generated nanoparticles are detected using *in situ* methods in the high temperature post flame region. Therefore, combustion generated nanoparticles are not exclusively formed by condensation of semivolatile species as their temperature significantly reduces in the exhaust system. The observation that the coagulation rate of d<3 nm particles is 2-3 orders of magnitude lower than that of soot suggests that they may survive through the exhaust system, and may account for the d<3 nm particles sometimes observed in the exhausts of practical combustion systems. The coagulation rate for d<3 nm particles depends strongly on the size, concentration, and temperature of the particles as well as the polarizability of the chemical structures comprising the particle. If the dilution conditions of exhaust increase significantly the rate of coagulation, d<3 nm particles may grow to the d=3-10 nm size range, and would therefore, be in the size range of detection by commercially available particle sizing instruments. This is an alternative explanation for the origin of observed nanoparticles in the exhaust of practical systems. Most studies conclude that observed nanoparticles in the exhaust are condensed semivolatile species since they depend greatly on the conditions of the dilution process, but the rate of condensation of semivolatiles and rate of coagulation of d<3 nm particles would be expected to change in the same way for a given sampling change. Table 2 illustrates this point by comparing the effects of various sampling changes expected for condensation of semivolatiles and coagulation of d<3 nm particles with the observed changes in nanoparticle (3<d<10 nm) concentration presented at this conference by various research groups world wide. Further work is needed to determine the extent to which nanoparticles are a result of condensation in the exhaust or products of coagulation of d<3 nm particles.

Table 2: Effect of sampling conditions on condensation or coagulation and observed changes in nanoparticle concentration.

change in sampling conditions[1]	Condensation of semivolatiles	Rate of coagulation of d<3 nm particles	Observed change in nanoparticle (d > 3 nm) concentration
Increase dilution ratio (increases temperature decreases concentration)	⬆ (Temperature) ⬇(Concentration)	⬆ (Temperature) ⬇(Concentration)	⬆ (Temperature) ⬇(Concentration)
Reduce temperature	⬆	⬆	⬆
Increase residence time	⬆	⬆	⬆
Use of thermal denuder	⬇	⬇	⬇
Remove large particles(reduces the total surface area and concentration of colliding particles)	⬆	⬆	⬆

[1]Results presented at the 5th ETH Conference on Nanoparticle-Measurement in Zurich, 2001.

UV-visible extinction spectra allow simultaneous measurement of soot and d<3 nm particles, and this technique was presented as a proof of concept for 3 practical systems: a stationary burner, and a gasoline and diesel engine. The results show that large stationary burners run in conditions designed to eliminate soot formation emit nanoparticles. Both gasoline and diesel engines are large potential sources of nanoparticles. A bimodal particle distribution (nanoparticles and soot) was observed in the exhaust of a diesel engine while only d<3 nm particles were detected in the gasoline engine exhaust. The results indicate that combustion systems running slightly fuel rich of stoichiometry, designed to reduce soot particles, likely produce large number concentrations of much smaller d<3 nm particles. The implications of emitted nanoparticles as opposed to soot particles are not yet understood, but their small size and affinity for water suggests that they may play a role on human and environmental health and should be considered in future studies.

Acknowledgements

References

[1] D'Alessio, A.; D'Anna, A.; Gambi, G.; Minutolo, P. *J. Aerosol Sci.* **29**, 397-409, 1998.
[2] Vander Wal, R. L. *Combustion and flame* **112**, 607-616, 1998.
[3] Dobbins, R. A.; Subramaniasivam, H. In *Soot Formation in Combustion*; Bockhorn, H., Ed.; Springer-Verlag: Heidelberg, 1994, pp 290-301.
[4] McEnally, C. S.; Koylu, U. O.; Pfefferle, L. D.; Rosner, D. E. *Combustion and Flame* **109**, 701-720, 1997.
[5] Minutolo, P.; Gambi, G.; D'Alessio, A.; Carlucci, S. *Atmos. Environ.* **33**, 2725-2732, 1999.
[6] Borghese, A.; Merola, S. S. *Applied Optics* **37**, 1-7, 1998.
[7] Kee, R. J.; Rupley, F. M.; Meeks, E.; Miller, J. A., Chemkin III: A Fortran chemical kinetics package for the analysis of gas phase chemical kinetics and plasma kinetics, 1989.
[8] Joutsenoja, T.; D'Anna, A.; D'Alessio, A.; Nazzaro, M. I. *Applied Spectroscopy* **55**, 130-135, 2001.
[9] Barone, A. C.; D'Alessio, A.; D'Anna, A. *submitted to Combustion and Flame* , 2001.
[10] Sgro, L. A.; Minutolo, P.; Basile, G.; D'Alessio, A. *Chemosphere* **42**, 671-680, 2001.
[11] Kaufman, S. L. *J. Aerosol Sci.* **29**, 537-552, 1998.
[12] Kaufman, S. L. *J. Aerosol Sci.* **30**, S821-S822, 1999.
[13] Fernandez de la Mora, J.; de Juan, L.; Eichler, T.; Rosell, J. *Trends in Anal. Chem.* **17**, 328-339, 1998.
[14] Gamero-Castano, M.; de la Mora, J. F. *J. Aerosol Sci.* **31**, 757-772, 2000.
[15] Seto, T.; Okuyama, K.; de Juan, L.; Fernandez de la Mora, J. *J. Chem. Phys.* **107**, 1576-1585, 1997.
[16] Gamero-Castano, M.; de la Mora, F. *Anal. Chim. ACTA* **406**, 67-91, 2000.
[17] Sgro, L. A. , 24th Event of the Italian Section of the Combustion Institute, S. Margherita Ligure, Italy, September 16-19 , 2001.
[18] Minutolo, P.; Gambi, G.; D'Alessio, A. *Proc. Combust. Inst.* **27**, 1461-1469, 1998.
[19] Minutolo, P.; Gambi, G.; D'Alessio, A.; D'Anna, A. *Combustion Science and Technology* **101**, 311-325, 1994.
[20] Basile, G.; Minutolo, P.; D'Anna, A.; D'Alessio, A. *submitted to Measurement Science and Technology* , 2001.
[21] Narsimhan, G.; Ruckenstein, E. *Journal of Colloid and Interface Science* **104**, 344-369, 1985.
[22] Merola, S. S.; Gambi, G.; Allouis, C.; Beretta, F.; Borghese, A.; D'Alessio, A. *Chemosphere* **42**, 827-834, 2001.
[23] Borghese, A.; Merola, S. S. *Proc. Combust. Inst.* **27**, 2101-2109, 1998.